Available online at www.sciencedirect.com
ScienceDirect
Polymer 48 (2007) 318–329
polymer
www.elsevier.com/locate/polymer

Novel low-κ polyimide/mesoporous silica composite films: Preparation, microstructure, and properties

Jingjing Lin, Xiaodong Wang*

Key Laboratory of Beijing City on Preparation and Processing of Novel Polymer Materials, School of Materials Science and Engineering, Beijing University of Chemical Technology, P.O. Box 61, Beijing 100029, People's Republic of China

Received 4 August 2006; received in revised form 20 October 2006; accepted 31 October 2006
Available online 27 November 2006

Abstract

A series of novel low-dielectric constant (low-κ) polyimide (PI) composite films containing the SBA-15 or the SBA-16-type mesoporous silica were successfully prepared via in situ polymerization and following thermal imidization. Their morphologies, dielectric constants, and thermal and dynamic mechanical properties were investigated. It is found that the dielectric constants of the composite films can be reduced from 3.34 of the pure PI to 2.73 and 2.61 by incorporating 3 wt% SBA-15 and 7 wt% SBA-16, respectively. The reduction of the dielectric constant is attributed to the incorporation of the air voids ($\kappa = 1$) stored within the mesoporous silica materials, the air volume existing in the gaps on the interfaces between the mesoporous silica and the PI matrix, and the free volume created by introducing large-sized domains. The PI/mesoporous silica composite films prepared in this study also present stable dielectric constants across the wide frequency range and a good phase interconnection. The improvement of the thermal stability and dynamic mechanical properties of the PI film is achieved by incorporation of the mesoporous silica materials. The enhanced interfacial interaction between the surface-treated mesoporous silica and the PI matrix has led to the minimization of the deterioration of the mechanical properties. The incorporation of the mesoporous silica materials is a promising approach to prepare the low-κ PI films.

Keywords: Polyimide/mesoporous silica composite films; Dielectric constant; Microstructure

1. Introduction

In the past decade, miniaturized ultra large-scale integrated circuit (IC) chips and semiconductor devices with improving performance have become a main orientation in microelectronics industry and been pursued as a global trend. However, the technicians and engineers have to face lots of serious technological problems in IC designs, such as the resistance capacitance time delay, cross-talks, power dissipation, etc. Fortunately, these problems can be effectively resolved by using inter-dielectric materials with low-dielectric constant (low-κ) [1–3]. Besides having a low-κ value, inter-dielectric materials should possess good thermal stability, low moisture uptake, excellent radiation and chemical resistance, high mechanical strength, and good adhesion to semiconductor and metal substrate. Considering these requests, a variety of polymers have been reported as potential low-κ materials for use in the development of advanced IC chips, which include polyimides, hetero-aromatic polymers, polyaryl ethers, fluoropolymers, nonpolar hydrocarbon polymers, polysilsesquioxanes, etc. [4].

As a species of the most important high-performance polymers, polyimides (PIs) are well known for their high-temperature durability, good mechanical properties, excellent chemical and thermal stabilities, low thermal expansion coefficient, and low-dielectric constant. They have been widely used as inter-dielectric materials in microelectronics and large-scale IC industry, as electrical insulation for conventional appliances, and as functional materials for other industrial applications. However, with dielectric constants of about 3.1–3.5, the conventional PIs are insufficient for meeting the requirement

* Corresponding author. Tel./fax: +86 10 6441 0145.
E-mail address: wangxdfox@yahoo.com.cn (X. Wang).

0032-3861/$ - see front matter © 2006 Elsevier Ltd. All rights reserved.
doi:10.1016/j.polymer.2006.10.037

of microelectronic and insulating applications. In recent years, the preparation of PIs with low-κ and high performance has become one of the research focuses. There are several approaches to reduce the dielectric constant of PIs, which include incorporation of fluorinated substituents into polymers [5–8], thermal degradation of the labile block or graft chains in the PI copolymers [9–11], and introduction of air gaps into interconnected structures and nanopores into polymers [12,13]. Considering that the incorporation of air having a dielectric constant of about 1 can decrease the dielectric constant remarkably by resulting in porous structure, most studies were focused on the last two approaches. Fu et al. prepared nanoporous low-κ polyimide films via grafting poly(amide acid) (PAA) with thermally degradable side chains by a reversible addition-fragmentation chain-transfer-mediated process [14]. Zhang et al. incorporated the hollow silica tubes into polyimide through ultrasonic dispersion and in situ polymerization so as to reduce the total dielectric constant of the composites ($\kappa = 2.952$, containing 3 wt% nano-scale silica tubes) [15]. Chen et al. introduced methacrylated-poly(silsesquioxane) (POSS) into the polyimide matrix to generate a PI/POSS semi-IPN-like nanocomposite, which resulted in an steady decrease of the dielectric constant as the methacrylated-POSS content increases ($\kappa = 2.51$, containing 15 wt% methacrylated-POSS) [16]. Wang et al. synthesized poly[4′,4″-(hexafluoroisopropylidene)-bis(4-phenoxyaniline)4,4-(hexafluoroisopropylidene)diphthalic anhydride]–montmorillonite (MMT) nanocomposites from modified MMT and PAA, whose dielectric constant reached a value of 2.6 at temperature over 100 °C [17].

Recently, mesoporous silica materials have attracted considerable interests in applications of molecular sieves, catalysts, adsorbents, optical devices, and sensor devices due to their highly ordered and uniform mesoporosity [18]. Most importantly, the mesoporous silica films synthesized via a surfactant templating process could provide large pore sizes (5–30 nm), high porosities (45–75%) and controlled pore structures [19]. This makes it possible to introduce voids into the bulk so that the low-κ air ($\kappa = 1$) can be utilized to reduce the dielectric constant of the materials. Many studies showed that the mesoporous silica films have low-dielectric constants in the range of 1.42–2.1 [20–22], which is lower than most of other low-dielectric materials, such as silisequioxane based dielectric, fluorine doped silica film, carbon doped silica film, and organic polymer dielectrics [23]. The low-κ mesoporous silica films can meet the requirements of the new dielectric films with low-dielectric constant ($\kappa < 2.5$) for the applications in the microelectronics and the insulations. However, owing to the poor processability of the mesoporous silica films, it is difficult to endue them with low-dielectric constant, low moisture uptake, and high mechanical strength simultaneously [24]. Based on the low-dielectric constant of the mesoporous silica, incorporation of the mesoporous silica into the PIs would be expected to reduce the dielectric constant of the PIs.

In order to obtain the low-κ materials with good performance through a sample method, we develop a new approach in this study to prepare the low-κ PI composite films by incorporating the mesoporous silica into PI matrix to combine the low-dielectric constant of mesoporous silica and the excellent properties of PI. A significant reduction of the dielectric constants for the PI composite films can be achieved with this method. We also evaluate the influence of the mesoporous silica materials on the PI composite films on basis of the dielectric, thermal, dynamic mechanical and mechanical properties. This method provides a sample and effective means to prepare the low-κ PI composite films.

2. Experimental

2.1. Materials

Poly(ethylene oxide-*b*-propylene oxide-*b*-ethylene oxide) (EO_n-PO_m-EO_n) triblock copolymers, $EO_{20}PO_{70}EO_{20}$ (Pluronic P123) and $EO_{106}PO_{70}EO_{106}$ (Pluronic F127) were commercially obtained from BASF Company. Tetraethoxysilane (TEOS) used as silica source and (γ-aminopropyl)triethoxysilane (APTS) used as coupling agent were purchased from Aldrich Chemical Company. Pyromelltic dianhydride (PMDA), 4,4′-oxydianiline (ODA), and *N*,*N*′-dimethylacetamide (DMAc) were purchased from Beijing Chemical Reagent Company. All chemicals were of reagent quality and used as received.

2.2. Synthesis of mesoporous silica materials

Two kinds of typical mesoporous silica materials, SBA-15 and SBA-16, were firstly synthesized by templating with the $EO_{20}PO_{70}EO_{20}$ and the $EO_{106}PO_{70}EO_{106}$ triblock copolymers, respectively, via a sol–gel process. In a typical synthesis of SBA-15, 4.0 g of P123 was dissolved in 30 g of deionized water and 120 g of 2 mol/L HCl solution with stirring at 35 °C for 6 h. Then 8.5 g of TEOS was added into that solution with stirring at 35 °C for 24 h. The mixture was aged at 100 °C for 24 h without stirring. The solid products were collected by filtration, washed with water, and dried at room temperature in air. The resulting powders were calcined at 500 °C for 5 h to remove the template. In a typical synthesis of SBA-16, 2.0 g of F127 and 5.24 g of K_2SO_4 were dissolved in 60 g of 0.5 mol/L HCl solution with stirring at 38 °C for 6 h. Then 8.40 g of TEOS was added into that solution with stirring at 38 °C for 24 h. The other procedures are the same as those described in the synthesis of SBA-15.

2.3. Preparation of composite films

The mesoporous silica materials were first surface treated with coupling agent before use in the following way. The mesoporous silica was dispersed in 95 wt% ethanol solution under ultrasonic agitation for 30 min, and then the calculated amount of APTS was added to the mixture, stirred for 24 h with a magnetic stirrer at 30 °C. After the mixture was filtrated with Buchner funnel, the product was washed several times using ethanol and dried in the vacuum oven at room temperature.

PI/mesoporous silica composite films were prepared via a two-step pathway, involving the synthesis of PAA/mesoporous silica composites and the thermal imidization of the PAA/mesoporous silica composite films. In the first step, the calculated

amount of SBA-15 or SBA-16 and 30 ml of DMAc were added to a three-necked flask under ultrasonic agitation for 30 min, and then, 2.0 g of ODA was added into the three-necked flask with a mechanical stirrer and cooled in an ice-water bath. After the ODA was dissolved completely, 2.02 g of PMDA was added into the flask step by step until the viscosity of the system increased abruptly, and then the system was stirred for an additional 2 h at 0 °C. In the second step, about 10 g of the mixture solution was cast on a square glass plate (5 × 5 cm) to obtain the films. The films were initially heated to remove the solution at 80 °C for 4 h under 0.05 MPa pressure in a vacuum oven, prior to the imidization step. The imiding process was carried out in a high-temperature oven with a heating program from 25 °C to 300 °C for 5 h; from 25 °C to 135 °C for 1 h; at 135 °C for 1 h; from 135 °C to 300 °C for 2 h; at 300 °C for 2 h. Finally, the film was peeled off from the glass plate to obtain the homogeneous and smooth PI/mesoporous silica composite film with the thickness of 350 μm, which was used for measurements of the dielectric properties.

2.4. Characterizations

X-ray diffraction (XRD) patterns of SBA-15 and SBA-16 were recorded on a Japan Rigaku D/max-RC instrument with Cu Kα radiation operating at 40 kV and 50 mA at a scanning rate of 2°/min. Transmission electron microscopic (TEM) images were obtained by a Hitachi H-800 transmission electron microscope operating at 200 kV. The samples for TEM were prepared by dispersing a drop of the suspension of ground sample in ethanol on a Cu grid covered by carbon film. The nitrogen adsorption and desorption isotherms were measured at 77 K using Nova 4200e system. Before the adsorption measurements, the samples were outgassed under vacuum at 200 °C for 2 h. The data of diameter distribution were analyzed by Barrett–Joyner–Halenda (BJH) method.

Scanning electron microscopic (SEM) observation was performed on a Cambridge S250 scanning electron microscope. The morphologies of the mesoporous silica powders and the fracture surfaces of the PI/mesoporous silica composite films were determined from SEM images. The composite films were fractured firstly in liquid nitrogen and mounted on the sample stud by means of a double-sided adhesive tape for cross-sectional view study. A thin layer of gold was sputtered onto the cross-sectional surface prior to SEM observation. Transmission Fourier transform infrared (FTIR) spectra of the mesoporous silica materials and the treated ones were obtained using a Bruker Tensor-27 FTIR spectrometer with 30 scanning numbers. Solid-state NMR spectra were recorded on a Bruker AV-300 NMR instrument. ^{29}Si MAS spectra were measured at 59.2 MHz using 4 mm silicon nitride rotors spinning at 5 kHz.

The dielectric constants of the composite films were measured on a WY2851-type LCR bridge meter (Shanghai Wuyi electronics Co., Ltd., China) in the frequency range of 50 kHz to 1 MHz. Dynamic mechanical analysis (DMA) was performed by using a Perkin–Elmer 7E dynamic mechanical analyzer to evaluate the storage modulus and mechanical loss factor (tan δ) of the composite films over the temperature range from 50 °C to 420 °C at a heating rate of 5 °C/min. The frequency and the strain were set to 1 Hz and 0.5%, respectively. The specimen size was 30 × 6 × 0.1 mm in length, width, and thickness, respectively. Thermal gravimetric analysis (TGA) was performed on a Perkin–Elmer Pyrid-1 thermal gravimetric analyzer at a heating rate of 10 °C/min from 50 °C to 900 °C under a dry nitrogen atmosphere. The tensile properties were determined with an Instron-1185 universal testing instrument using a 1000 N load transducer according to the standard of ASTM D-638. Small dumb-bell shaped specimens with waist dimensions of 20 × 4 mm were used for tensile mechanical tests. All the tests were done at room temperature and five measurements were carried out for each data point.

3. Results and discussion

3.1. Microstructure and properties of the synthesized mesoporous silica

Two kinds of typical mesoporous silica materials, SBA-15 and SBA-16, were synthesized by templating with the $EO_{20}PO_{70}EO_{20}$ and $EO_{106}PO_{70}EO_{106}$ triblock copolymers as templates, respectively, via a sol–gel process. Fig. 1 shows the XRD patterns of SBA-15 and SBA-16. One can find a well-resolved single diffraction peak at $2\theta = 0.93°$ and 0.71°, respectively, as well as a series of broad diffraction peaks with low intensity for each mesoporous silica. Through the Bragg's law and the corresponding relationship between the cubic unit cell parameter and interplanar distance at different Miller indices, a two-dimensional (2D) hexagonal structure (*p6mm*) and a three-dimensional (3D) body-centered cubic structure (*Im3m*) could clearly be identified and assigned to SBA-15 and SBA-16, respectively. The TEM image in Fig. 2(a) confirms the ordered structure of SBA-15, and shows that the cylindrical pores are arranged in an ordered hexagonal array. From Fig. 2(b), the arrays of the ordered and uniform pores interconnection can be observed for SBA-16. Some mesoporous properties of SBA-15 and SBA-16 were obtained by the nitrogen

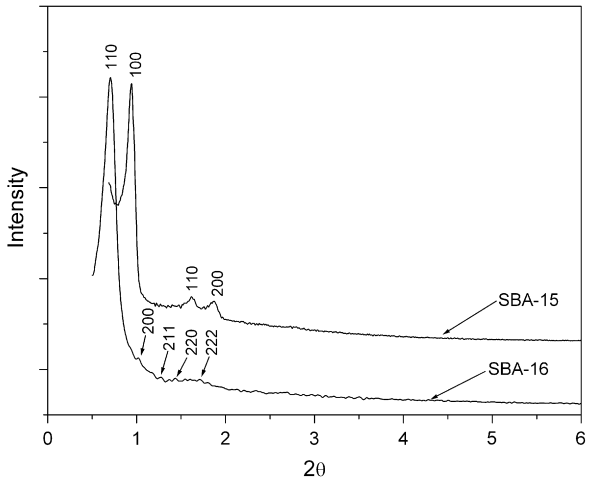

Fig. 1. X-ray diffraction patterns of the calcined mesoporous silica materials.

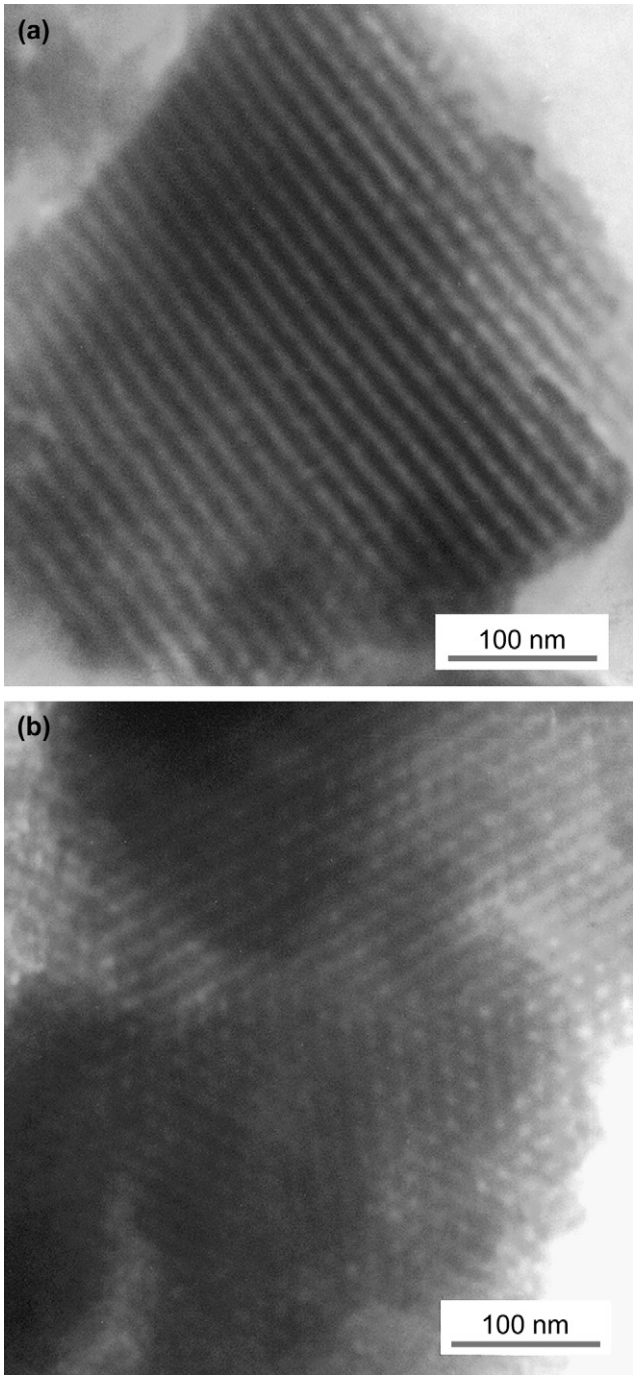

Fig. 2. TEM images of the mesoporous silica materials: (a) SBA-15 and (b) SBA-16.

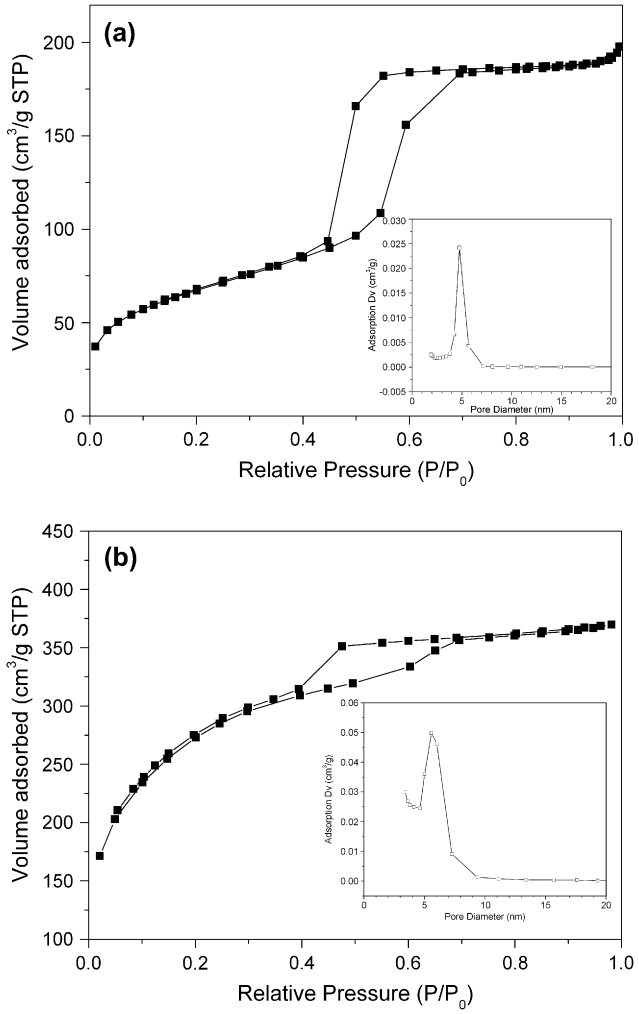

Fig. 3. Nitrogen adsorption–desorption isotherm and pore size distribution (the inset) plots for (a) SBA-15 and (b) SBA-16.

adsorption–desorption isotherms as shown in Fig. 3, which demonstrate typical Langmuir IV-type isotherms with a H_1 hysteresis loop assigned to the 2D hexagonal and a H_2 hysteresis loop assigned to the 3D cubic cage-like mesoporous structure, respectively [19,25]. Both SBA-15 and SBA-16 have small pore diameters of 5–6 nm with very narrow pore size distributions. Total pore volumes for SBA-15 and SBA-16 can also be calculated to be 1.12 cm^3/g and 0.68 cm^3/g in Brunauer–Emmett–Teller model. These important parameters indicate the amount of air voids stored in the mesoporous silica materials [26].

3.2. FTIR spectroscopy

The PI/mesoporous silica composite films were obtained through in situ polymerization of the mixture of PI precursors containing various amount of SBA-15 or SBA-16, and then was thermally imidized on a flat glass plate. However, the surface treatment should firstly be performed for mesoporous silica materials because of poor interfacial adhesion between the inorganic mesoporous silica and the organic PI matrix. In this study, we employed the APTS as coupling agent, which was capable of linking mesoporous silica covalently to the PI through silylation of mesoporous silica [27,28]. Two intensive absorption peaks at 1100 cm^{-1} and 790 cm^{-1} belonging to the asymmetric and symmetric stretching vibrations, respectively, corresponding to the Si–O–Si framework could be observed from the FTIR spectra of SBA-15 and SBA-16 as shown in Fig. 4. The wide absorption band at around 3450 cm^{-1} as well as the weak band at 968 cm^{-1} represents Si–OH stretching

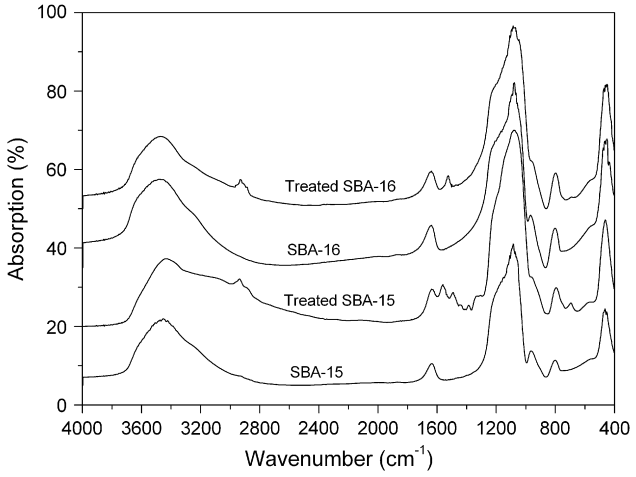

Fig. 4. FTIR spectra of the untreated and treated mesoporous silica materials.

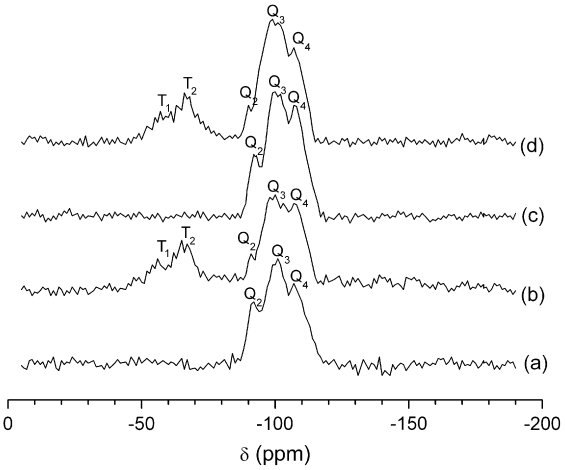

Fig. 5. ^{29}Si MAS NMR spectra of: (a) SBA-15, (b) APTS-treated SBA-15, (c) SBA-16, and (d) APTS-treated SBA-16.

and bending vibrations, respectively. Since the mesoporous silica materials we prepared have been synthesized through synergistic self-assembly between surfactant (triblock polymer) and silica source (TEOS) to form mesoscopically ordered composites, they were formed via a condensation of silanols along the micellar surface of the surfactant in an acidic media. It is expected that a large quantity of silanol groups should be detected on their inorganic walls. It is evident that the FTIR spectra of the mesoporous silica materials confirm these silanol groups (Si−OH). From the IR spectra of the treated SBA-15 and SBA-16 as shown in Fig. 4, a series of new absorption peaks are observed. The peaks at 2930 cm^{-1} and 1490 cm^{-1} correspond to the $-CH_2$ stretching absorption and the $-CH_2$ scissor vibration, respectively, while the peak at 1550 cm^{-1} is attributed to the absorption of $-NH_2$. These results indicate that the APTS has been chemically grafted onto the mesoporous silica materials through condensation between the silanol groups of the hydrolyzed APTS and those on the surface of the mesoporous silica.

The solid-state NMR spectra ^{29}Si CP-MAS NMR spectra were also collected to confirm the chemically grafted APTS onto the mesoporous silica materials through condensation, as shown in Fig. 5. It can be seen that the ^{29}Si MAS NMR spectrum of the SBA-15 silica is broad and dominated by three overlapping peaks (an intense peak at −100 ppm along with two shoulders at the chemical shifts of −90 and −108 ppm), indicating a close proximity of these silicon atoms to protons. Similar to the amorphous silica, the chemical shift at −108 ppm can be assigned to $Si(-O-Si)_4$ (Q_4) structural units, and the peaks at −100 and −90 ppm to $Si(-O-Si)_3-OH$ (Q_3) and $Si(-O-Si)_2(-OH)_2$ (Q_2) structural units, respectively [29,30]. The Q_4 structural units represent interlinked SiO_4 tetrahedrons in the interior of the mesoporous silica walls, while Q_3 and Q_2 structural units are present on the wall surface associated with silanol groups. The signals for these resonances can also be seen in the ^{29}Si MAS NMR spectrum of the APTS-treated SBA-15; however, the intensity of the resonance for Q_2 structural units weakens. In addition, other chemical shifts at −58 (T_1) and −67 ppm (T_2) could be observed upon incorporation of aminopropyl groups, and no peak appears at −45 ppm corresponding to the chemical shift of silicon in APTS, indicating the absence of free silane molecules physically adsorbed on the surface of the SBA-15. The appearance of the peaks at −58 and −67 ppm indicates the formation of new siloxane linkages (Si−O−Si) of aminopropylsilane silicon to the surface silicon atoms of the SBA-15. The relative high intensity of the peak at −67 ppm indicates that the incorporated aminopropyl groups are closely packed on the surface of the SBA-15. The results suggest that the surface silanol groups, which are associated with Q_2 structural units of the SBA-15 silica, are consumed and attached to aminopropylsilane via siloxanes [31,32]. Similar phenomena could be observed from the ^{29}Si MAS NMR spectra of the pure and the APTS-treated SBA-16. The mesoporous silica's surface bound APTS may further react with PAA during in situ polymerization process (the possible linking way is seen in Fig. 6) [27,33], and thus the enhanced interfacial adhesion between the mesoporous silica and the PI matrix can improve the incorporation of the mesoporous silica materials into PI.

3.3. Morphology of composite films

Fig. 7(a) and (b) shows the SEM images of the external morphologies of SBA-15 and SBA-16, respectively. It can be clearly observed that the SBA-15 and the SBA-16 exhibit a completely different morphology themselves, in which the SBA-15 displays a node-rod-like shape with around 10 μm in length. Furthermore, these node-rod-like sub-particles agglomerate each other and form clusters, which were resulted from the condensation of TEOS around the adjacent micelles of the template P123. On the other hand, the SBA-16 presents a very regular sphere with uniform sizes of 2−4 μm. The original morphologies of the mesoporous silica materials are determined by the colloidal phase separation mechanisms. The completely different morphology of SBA-15 and SBA-16 was due to their individual template used for synthesis.

Fig. 7(c)−(f) shows the SEM images of the fracture surface of the PI/mesoporous silica composite films, and the SEM

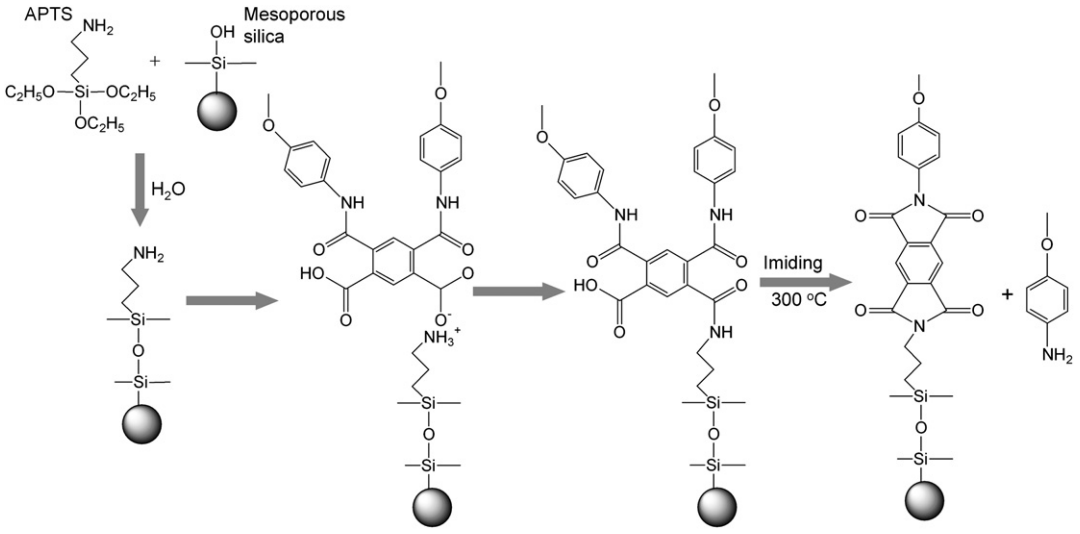

Fig. 6. Scheme of possible reaction between the mesoporous silica's surface bound APTS and PAA.

image of fracture surface of the pure PI film as reference is shown in Fig. 7(g). It is noted that the fracture surface of the pure PI film illustrates some large plastic deformation, indicating a typical tough fracture behavior. One can also clearly observe distribution of the mesoporous silica in the composite film from the fracture surface, due to the contrast of these two materials. Owing to the initial agglomeration of the SBA-15, it can only be dispersed as macro-sized aggregates of the node-fiber-shaped materials in the PI matrix even with the aid of surface treatment and ultrasonic vibration, as shown in Fig. 7(c) and (d). However, one can find that SBA-16 is dispersed uniformly as individual spherical particles in the PI matrix for the composite film containing 5 wt% SBA-16, as shown in Fig. 7(e). Moreover, when the content of SBA-16 reaches 10 wt%, the individual particles aggregate together [see Fig. 7(f)], indicating a poor dispersion for SBA-16 at higher content.

3.4. Dielectric properties

Fig. 8 displays the variety of the dielectric constants measured at the frequency of 1.0 MHz as a function of the mesoporous silica content. It is very interesting to notice that the dielectric constant reduces from 3.34 to around 2.9 by incorporating 1 wt% SBA-15 or SBA-16 into the composite film, and the dielectric constant gradually decreases with increasing the amount of the mesoporous silica materials continuously. For the composite film containing 3 wt% SBA-15, the dielectric constant exhibits a minimum value of 2.73. However, the dielectric constant of the PI/SBA-16 composite films continuously decreases until the content of SBA-16 reaches 7 wt%, at which the composite film achieves a minimum dielectric constant ($\kappa = 2.61$). After the content of mesoporous silica exceeds the characteristic point, where a minimum dielectric constant was obtained, the dielectric constants for both the PI/SBA-15 and the PI/SBA-16 composite films begin to increase with increasing the amount of mesoporous silica. Furthermore, the PI/SBA-15 composite films present a more great increment of the dielectric constant than the PI/SBA-16 ones. All of the measurements have been repeated five times and the deviations of the testing data were controlled with ± 0.05. Therefore, it is believable that the reduction of the dielectric constant is resulted from the incorporation of air voids ($\kappa = 1$) when the mesoporous silica materials are introduced into the composite films.

As we know, there are mainly three models to predict the dielectric constant of the dual-component composite: Maxwell–Garnett, Bargeman, and Yamada models. The Maxwell–Garnett equation was widely used to calculate the dielectric constant of polymeric composites. And the Yamada model was mainly used to calculate the dielectric constant at different electric field strengths, so the depolarization factor should be considered based on the electric field effect with a complicated equation [34]. It is obvious that the Yamada model is outside of the target of our research on the PI/mesoporous silica composite films. Although there are three components including PI, silica (SiO_2), and air in the composite film, the reduction of the dielectric constant is mainly attributed to the implantation of air alone with the mesoporous silica materials. Therefore, the composite film can be firstly considered as a dual-component system (the PI and the mesoporous silica). The theoretical dielectric constants of the composite films can be predicted by using Maxwell–Garnett equation [35]:

$$\frac{\kappa - \kappa_p}{\kappa + 2\kappa_p} = \phi_m \frac{\kappa_m - \kappa_p}{\kappa_m + 2\kappa_p} \quad (1)$$

where κ_p and κ_m are the dielectric constants of the PI and the mesoporous silica, respectively, κ the predicted dielectric constant of the composite, and ϕ_m the volume fraction of the mesoporous silica. The dielectric constants of mesoporous silica materials can also be calculated by Eq. (1) based on the total pore volume, corresponding to the air volume stored within mesoporous silica. All of the calculated dielectric constants as well as the measured ones for reference are listed in Table 1. It can be noted that the measured dielectric constants

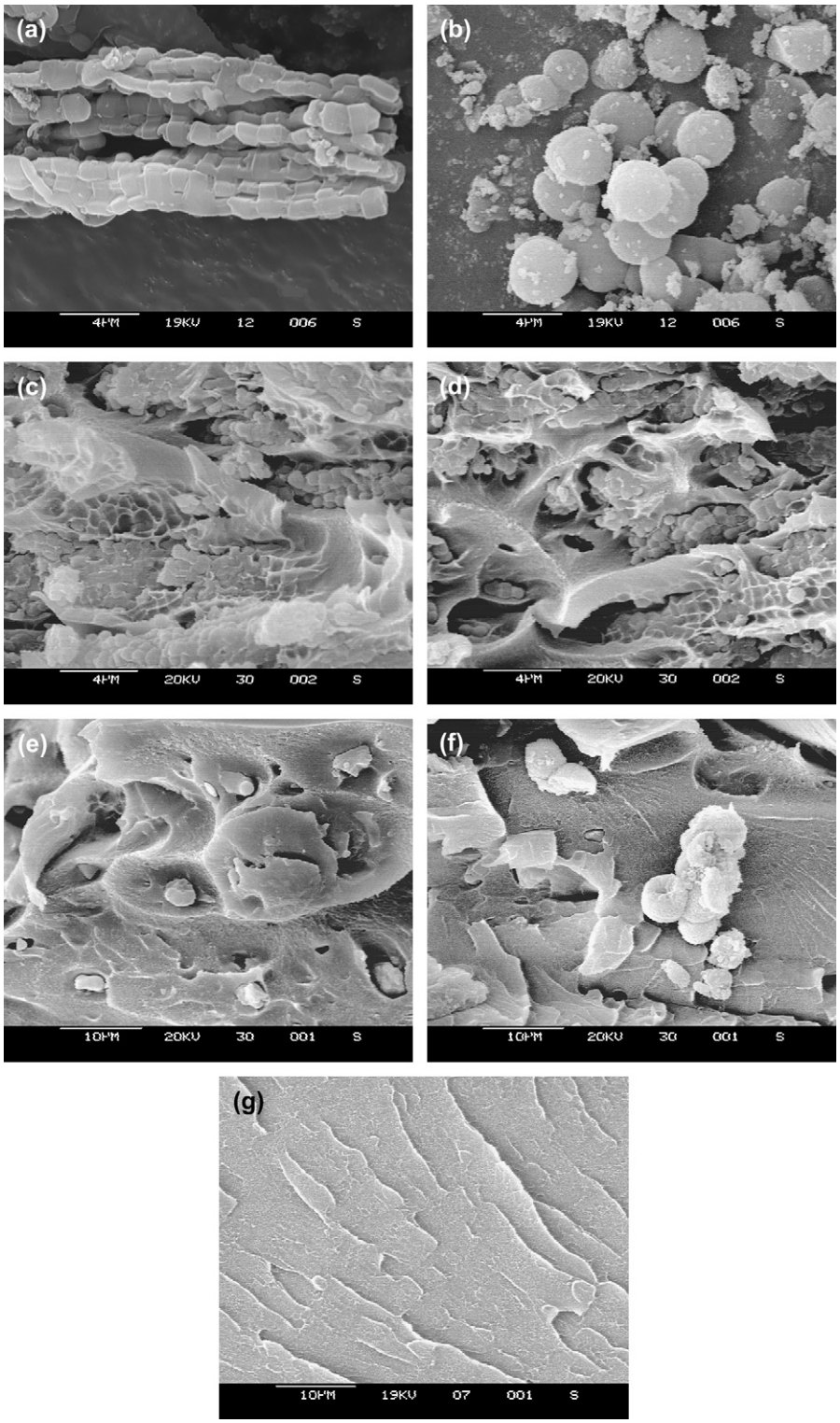

Fig. 7. SEM images of mesoporous silica and the PI/mesoporous silica composite films: (a) SBA-15, (b) SBA-16, (c) the composite films containing 5 wt% SBA-15, (d) the composite films containing 10 wt% SBA-15, (e) the composite films containing 5 wt% SBA-16, (f) the composite films containing 10 wt% SBA-16, and (g) the pure PI film.

of the composite films differ remarkably from the theoretical data, which are much greater for the composite with the same amount of SBA-15 or SBA-16. The results show that the difference of the pore volumes in the mesoporous silica exactly plays an important role to decrease the dielectric constant of the composites films. Furthermore, the theoretical data decrease continuously with increasing the amount of the mesoporous silica, but the measured values present a minimum at a characteristic concentration of the mesoporous silica. This implies that the reduction of the dielectric constants is not only

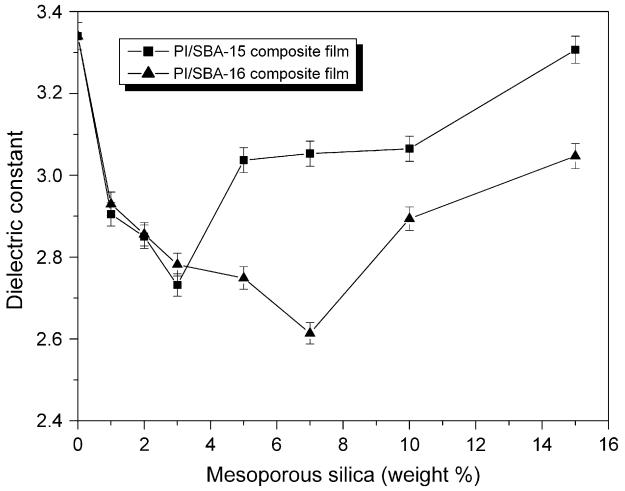

Fig. 8. Dielectric constants of the PI/mesoporous silica composite films at a frequency of 1 MHz as a function of the mesoporous silica content.

attributed to the air volume stored within the mesoporous silica materials.

In order to explore the reason why this deviation occurs, we calculated the air volume percentages of the composite, which only include the air volume within the mesoporous silica materials, and total air volume in the composite by using Bruggeman's model. Assuming there are only three phases in the composite as mentioned previously, the total volume percentage in the composite can be calculated by using Bruggeman's equation [15] for three-component composite:

$$\phi_p\left(\frac{\kappa_p-\kappa}{\kappa_p+2\kappa}\right)+\phi_s\left(\frac{\kappa_s-\kappa}{\kappa_s+2\kappa}\right)+\phi_a\left(\frac{\kappa_a-\kappa}{\kappa_a+2\kappa}\right)=0 \quad (2)$$

where κ_p, κ_s, and κ_a, are the dielectric constants of the PI, the silica and the air, respectively, κ the measured dielectric constant of the composite, and ϕ_p, ϕ_s, and ϕ_a the volume fractions of the PI, the silica and the air, respectively. All of the calculated results are also listed in Table 1. It is clearly noticed that the actual total air volume in the composite is much greater than the air volume stored within mesoporous silica materials. These air voids may exist in the gaps on the interfaces between the mesoporous silica and the PI matrix, and the free volume created by introducing macro-sized domains [36]. From Fig. 7, it is found that the air voids around the mesoporous silicas really exist, which can drastically decrease the dielectric constant of the composite films. Moreover, even the air volume in the pores created during the mixing process should also be considered to contribute to the total air volume. Therefore, the reduction of the dielectric constant is contributed by the whole air voids created by incorporating the mesoporous silica, which includes the air volume stored within the mesoporous silicas, the air void coming from the gaps on the interfaces between the mesoporous silicas and the PI matrix, and the free volume created by introducing macro-sized domains. One may also find that total air volume presents a maximum at a characteristic concentration of the mesoporous silica, and begins to decrease with increasing the amount of the mesoporous silica continuously in terms of the Bruggeman's model. This result indicates that the incorporation of too much mesoporous silica results in its aggregation and poor dispersion, a decrease of the air volume, and thus an increase of the dielectric constant. It is also noteworthy that both the internal structures and the external morphologies of the mesoporous silicas reveal a significant effect on the variation trends of the dielectric constant as a function of the content of the mesoporous silica. As mentioned previously, the SBA-15 has a larger pore volume than the SBA-16, so it results in a lower dielectric constant for the composite films than the SBA-16. However, the SBA-15 does not exhibit any superiority than the SBA-16 at a higher content in the composite films, as shown in Fig. 8. Apparently, the external morphologies of two kinds of mesoporous silicas dominate the dielectric constants of the composite films with much higher content of mesoporous silica, because the characteristic morphology of the mesoporous silica affects its distribution in the PI matrix significantly, and then determines the free volume and the gaps on the interfaces between the PI and the mesoporous silica. As a result, the composite films containing higher content of SBA-15 exhibit a higher dielectric constant than those containing SBA-16.

Fig. 9 shows the frequency dependence of the dielectric constant of the pure PI and its composite films in the frequency range of 50–1000 kHz. Although the variation of the dielectric constants of the PI composite films as a function

Table 1
Measured and theoretical dielectric constants, and air volume percentages in the composite films calculated by corresponding models

Materials	Measured dielectric constant at 1 MHz	Theoretical dielectric constant[a]	Air volume stored within mesoporous silica in composites[b] (v/v%)	Total air volume in composites[c] (v/v%)
PI	3.34	–	–	–
Silica (SiO_2)	4.00	–	–	–
Air	1.00	–	–	–
1 wt% SBA-15/PI	2.91	3.25	1.58	14.63
2 wt% SBA-15/PI	2.85	3.18	3.13	16.62
3 wt% SBA-15/PI	2.73	3.10	4.63	20.18
5 wt% SBA-15/PI	3.04	2.95	7.54	10.40
7 wt% SBA-15/PI	3.05	2.82	10.32	10.33
10 wt% SBA-15/PI	3.07	2.63	14.26	–
15 wt% SBA-15/PI	3.31	2.36	20.28	–
1 wt% SBA-16/PI	2.93	3.29	0.97	13.78
2 wt% SBA-16/PI	2.86	3.22	1.92	16.41
3 wt% SBA-16/PI	2.78	3.16	2.86	19.05
5 wt% SBA-16/PI	2.75	3.05	4.72	20.39
7 wt% SBA-16/PI	2.61	2.94	6.53	25.28
10 wt% SBA-16/PI	2.89	2.79	9.17	15.98
15 wt% SBA-16/PI	3.05	2.56	13.37	–

[a] The theoretical dielectric constants were calculated by using Maxwell–Garnett equation.
[b] The air volume stored within mesoporous silica in composites (volume fraction) was calculated by using the data from the nitrogen adsorption–desorption experiment along with calculation in BET mode.
[c] Total air volume in composites (volume fraction) was calculated according to Bruggeman's model.

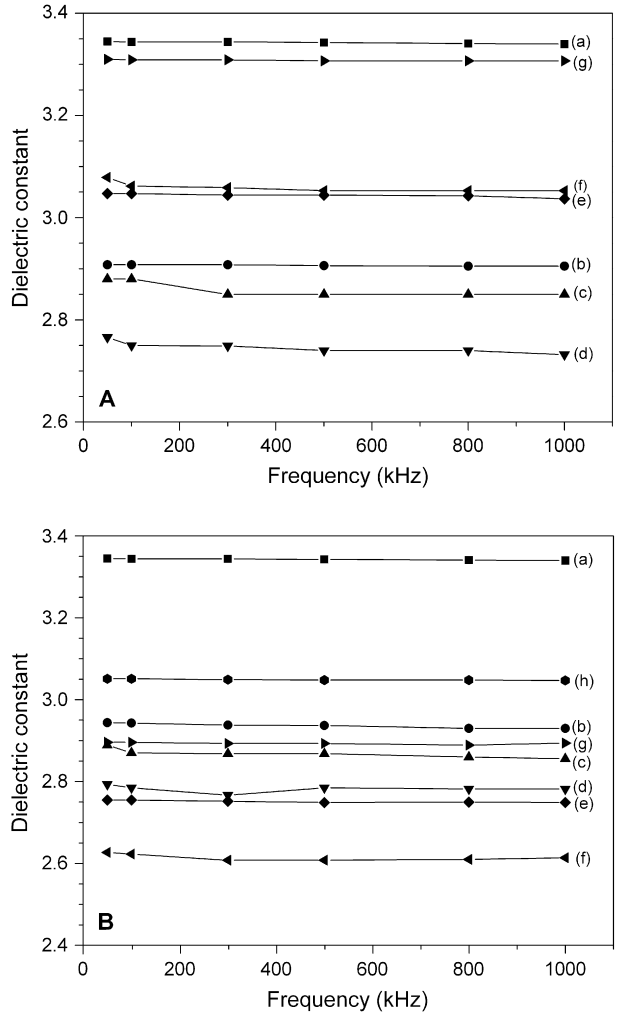

Fig. 9. Frequency dependence of dielectric constants for: (A) PI/SBA-15 and (B) PI/SBA-16 composite films with mesoporous silica content of (a) 0 wt%, (b) 1 wt%, (c) 2 wt%, (d) 3 wt%, (e) 5 wt%, (f) 7 wt%, (g) 10 wt%, and (h) 15 wt%.

of the SBA-15 or the SBA-16 content is identical to the trend shown in Fig. 8, the dielectric constants for both pure PI and its composite films are almost independent of the frequency except at very low frequency, where some dielectric constants are fairly higher. One can find that the dielectric constant only decreases slightly with increasing frequency while temperature is kept constant at room temperature. It is well known that the dielectric constant of materials tends to decrease gradually with increasing the frequency, because the response of the electronic, atomic, and dipolar polarizable units varies with frequency. This behavior can be attributed to the frequency dependence of the polarization mechanisms [37]. Therefore, the magnitude of the dielectric constant for a polymer like PI is determined by the ability of the polarizable units to orient fast enough to keep up with the applied alternating current electric field. The orientational polarization decreases while the frequency increases, as the orientation of dipole moments needs a longer time than the electronic and ionic polarization. This results in a reduction of the dielectric constant. The PI/mesoporous silica composite films prepared in this study exhibit the stable dielectric constants across the wide frequency range, which are highly preferred for many microelectronic applications.

3.5. Thermal properties

The effect of SBA-15 and SBA-16 on the thermal degradation of the PI was studied using TGA in the temperature range of 50–900 °C. From the TGA curves shown in Fig. 10, one can observe that the thermal degradation of the pure PI and its composite films in this temperature range occurs through one degradation step, which indicates that a good phase interconnection between the mesoporous silica and PI matrix, and successful chemical graft of the APTS onto the mesoporous silica materials. The TGA curves also indicate that water or solvent has been successfully removed from the PI film and the composite films because there is no weight loss below 100 °C. It is clearly shown in Fig. 10 that the thermal stability of the PI is increased by incorporation of the mesoporous silica materials in terms of the weight residues above 750 °C. The increase in weight residues above 750 °C suggests successful incorporation of higher amount of silica into the composite films and ultimately increases the thermal stability. This improvement in the thermal stability of composite films mainly comes from the enhanced interaction/chemical bonding between the PI matrix and the mesoporous silica [38]. Furthermore, it may also be assumed that the thermal stability of organic materials can be improved by introducing inorganic components such as silica, on the basis of the fact that these materials have inherently good thermal stability [39].

3.6. Dynamical mechanical properties

Fig. 11 presents the dynamic mechanical spectra of the pure PI and its composite films expressed in terms of storage modulus as a function of temperature. One can observe that the storage moduli of the composite films are greater than that of the pure

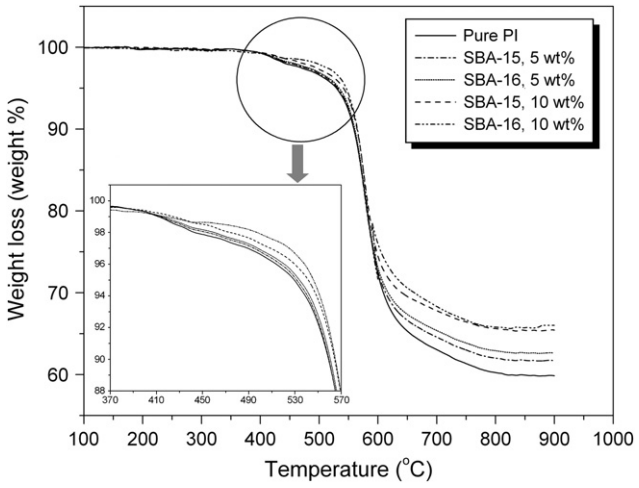

Fig. 10. TGA thermograms of the pure PI and its composite films in nitrogen atmosphere.

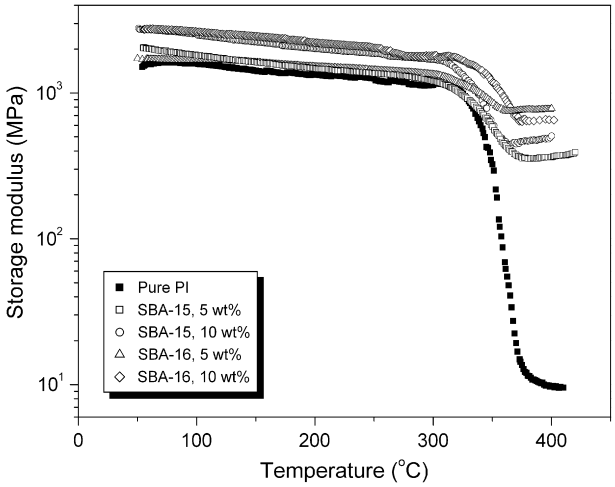

Fig. 11. Storage moduli of the pure PI and its composite films as a function of temperature.

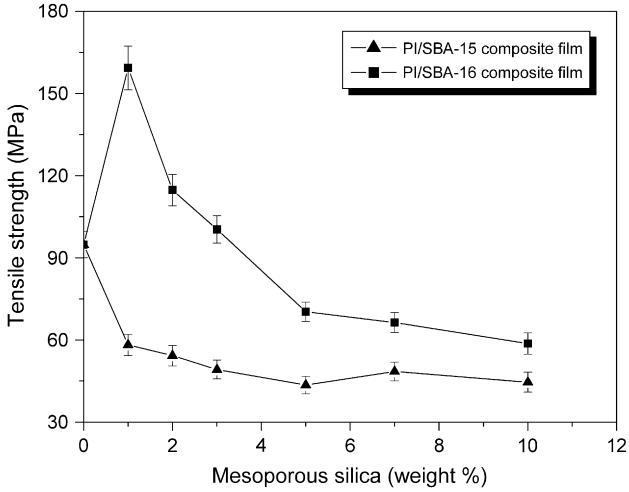

Fig. 13. Tensile strength of the PI/mesoporous silica composite films as a function of the mesoporous silica content.

PI, especially at the high temperature of over 380 °C, and the composite films containing greater amount of the mesoporous silica have higher storage moduli. One can note a significant difference in the storage modulus between the composite films containing the SBA-15 and the SBA-16, and the composite films containing the SBA-16 have much higher moduli than those containing the SBA-15. This phenomenon may be resulted from the large domain size and poor dispersion of the SBA-15. It can be also seen from Fig. 12 that the pure PI and its composite films exhibit a well-resolved single relaxation peak, corresponding to the glass transition temperature (T_g). Furthermore, the relaxation peaks of the composite films occur at a temperature of about 3–5 °C higher than that of pure PI. It is still clearly observed that the T_gs of the composite films (based on the maximum of the mechanical loss peak) increase slightly with increasing the content of the mesoporous silica. These results indicate that the presence of the fully elastic inorganic phase can result in a decrease of the viscous response of the visco-elastic PI [40], and also reflect an improved phase interconnection and a good interfacial adhesion between the phases with the aid of coupling agent.

3.7. Mechanical properties

The tensile strength, elongation at break, and Young's modulus of the PI/mesoporous silica composite films as a function of the mesoporous silica content are plotted in Figs. 13–15, which indicate that the content and morphology of the mesoporous silica materials have significant effects on the mechanical properties of the PI/mesoporous silica composite films. The tensile strength and Young's modulus of the PI/SBA-16 composite films are improved to 159.4 MPa and 3555 MPa from 94.8 MPa and 2554 MPa of the pure PI, respectively, by incorporating 1 wt% SBA-16. However, both of them decrease rapidly, as the content of SBA-16 increases continuously. The elongation at break of the composite films also presents a sharp decrease with the addition of 1 wt% SBA-16. However, it increases slightly with continuous increase of

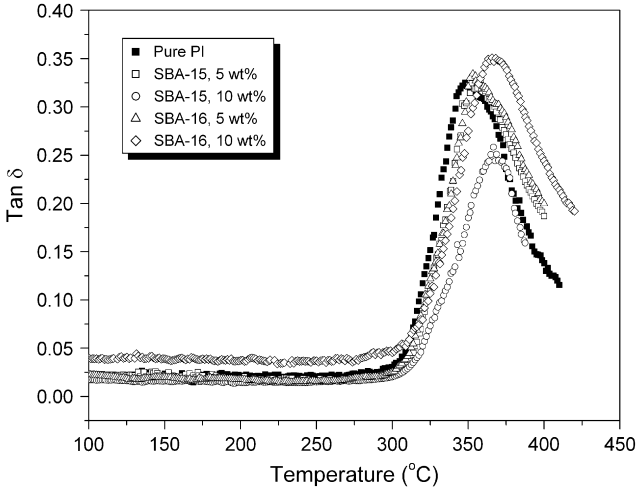

Fig. 12. Mechanical loss factors (tan δ) of the pure PI and its composite films as a function of temperature.

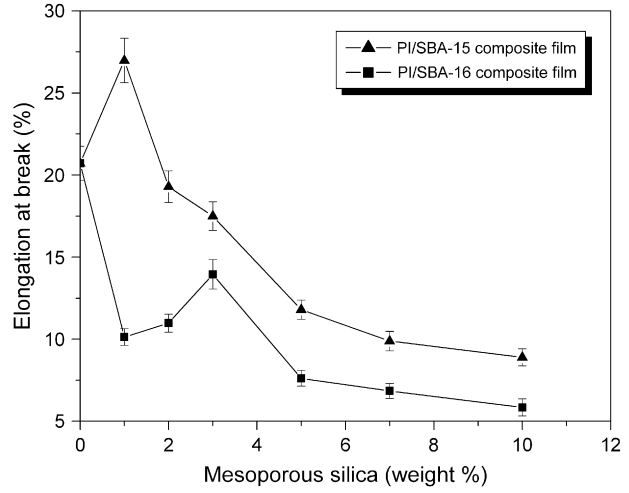

Fig. 14. Elongation at break of the PI/mesoporous silica composite films as a function of the mesoporous silica content.

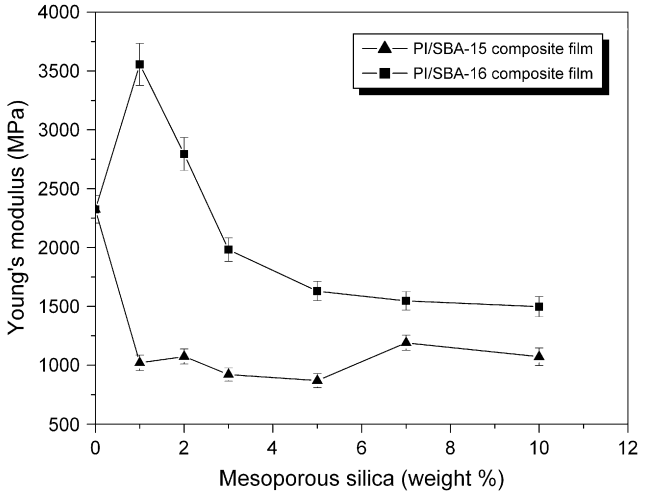

Fig. 15. Young's modulus of the PI/mesoporous silica composite films as a function of the mesoporous silica content.

SBA-16 until the concentration of SBA-16 reaches 3 wt%, and then begins to decrease. On the other hand, one may also find that the tensile strength and Young's modulus of the PI/SBA-15 composite films continue to decrease with increasing the SBA-15 content, but the elongation at break is only improved for the composite film containing 1 wt% SBA-15 and begins to decrease with continuously increasing SBA-15 content. Furthermore, the PI/SBA-15 composite films present much lower tensile strength and Young's modulus than the PI/SBA-16 ones, indicating that SBA-15 has much more negative effects on the mechanical properties than SBA-16.

One can clearly distinguish the quite different mechanical variation trends as a function of the content of mesoporous silica for SBA-15 and SBA-16. It is evident that this phenomenon is resulted from the characteristic morphologies of these two mesoporous silica, which resulted in a different distribution of the mesoporous silica in PI matrix. It is also understandable that the improvement of the mechanical properties for the composite films is closely related to the morphology and dispersion of the mesoporous silica. It is clear that the small amount of loading like 1 wt% SBA-16 can generate a better dispersion, resulting in the improved mechanical properties. The natural agglomeration makes SBA-15 poorly dispersed in the PI matrix, and thus results in reduction of the mechanical properties. The similar arguments have already been reported in the literatures [41–44]. It is noteworthy that the enhanced interfacial adhesion of the mesoporous silica and the PI matrix should be addressed for the improvement of the mechanical properties, with regard to the surface treatment of the mesoporous silica by APTS as a coupling agent. It has been well established that phase compatibilization between the mesoporous silica and the PI matrix can be achieved by chemical reaction between the mesoporous silica's surface bound APTS and the PI matrix. The enhanced interfacial adhesion of the resultant composite films using coupling agent may govern overall properties of final composite films. In this work, it can be deduced that the mesoporous silica's surface bound APTS plays a vital role to induce some chemical bonding as well as strong interaction such as hydrogen bonding between the mesoporous silica and the PI matrix [45]. As a result, the deterioration of the mechanical properties can be minimized, and some improvements are gained.

4. Conclusion

A series of the novel PI composite films containing the SBA-15 or the SBA-16 type mesoporous silica were successfully prepared via the in situ polymerization and following thermal imidization. The dielectric constants of the PI composite films can be reduced from 3.34 of the pure PI to 2.73 and 2.61 by incorporating 3 wt% SBA-15 and 7 wt% SBA-16, respectively. The reduction of the dielectric constant is attributed to the incorporation of the air voids ($\kappa = 1$) stored within the mesoporous silica materials, the air volume existing in the gaps on the interfaces between the mesoporous silica and the PI matrix, and the free volume created by introducing large-sized domains. The SBA-16 has a more significant effect on reduction of the dielectric constant than the SBA-15 because of its smaller domain size and more uniform distribution in the matrix. The PI/mesoporous silica composite films prepared in this study also present stable dielectric constants across the wide frequency range and a good phase interconnection. The thermal stability and dynamic mechanical properties of the PI film can be improved by incorporation of the mesoporous silica materials. The enhanced interfacial interaction between the surface-treated mesoporous silica and the PI matrix can lead to the minimization of the deterioration of the mechanical properties. The incorporation of the mesoporous silica materials is a promising approach to reduce the dielectric constant.

Acknowledgements

The authors greatly appreciate financial support from the National Nature Science Foundation of China (Grant No.: 50573006).

References

[1] Ree MH, Yoon JW, Heo KY. J Mater Chem 2006;16:685–97.
[2] Huang YQ, Economy J. Macromolecules 2006;39:1850–3.
[3] Deligoz H, Ozgumus S, Yalcinyuva T, Yildirim S, Deger D, Ulutas K. Polymer 2005;46:3720–9.
[4] Ree M. Macromol Res 2006;14:1–33.
[5] Li HS, Liu JG, Rui JM, Fan L, Yang SY. J Polym Sci Part A Polym Chem 2006;44:2665–74.
[6] Myung BY, Ahn CJ, Yoon TH. Polymer 2004;45:3185–93.
[7] Miyagawa T, Fukushima T, Oyama T, Iijima T, Tomoi M. J Polym Sci Part A Polym Chem 2003;41:861–71.
[8] Madhra MK, Salunke AK, Banerjee S, Prabha S. Macromol Chem Phys 2002;203:1238–48.
[9] Su YC, Chen WC, Ou KL, Chang FC. Polymer 2005;46:3758–66.
[10] Chen YW, Wang WC, Yu WH, Kang ET, Neoh KG, Vora RH, et al. J Mater Chem 2004;14:1406–12.
[11] Chen YW, Wang W, Yu WH, Yuan ZL, Kang ET, Neoh KG, et al. Adv Funct Mater 2004;14:471–8.
[12] Chen YW, Kang ET. Mater Lett 2004;58:3716–9.
[13] Leu CM, Chang YT, Wei KH. Chem Mater 2003;15:3721–7.

[14] Fu GD, Zong BY, Kang ET, Neoh KG. Ind Eng Chem Res 2004; 43:6723–30.
[15] Zhang YH, Lu SG, Li YQ, Dang ZM, Xin JH, Fu SY, et al. Adv Mater 2005;17:1056–9.
[16] Chen WY, Ko SH, Hsieh TH, Chang FC, Wang YZ. Macromol Rapid Commun 2006;27:452–7.
[17] Wang HW, Dong RX, Chu HC, Chang KC, Lee WC. Macromol Chem Phys 2005;94:42–51.
[18] Yang PD, Zhao DY, Margoless DI, Chmelka BF, Stucky GD. Nature 1998;396:152–5.
[19] Zhao DY, Feng JL, Huo QS, Melosh N, Fredrickson GH, Chmelka BF, et al. Science 1998;279:548–52.
[20] Baskaran S, Liu J, Domansky K, Kohler N, Li XH, Coyle C, et al. Adv Mater 2000;12:291–4.
[21] Yang CM, Cho AT, Pan FM, Tsai TG, Chao KJ. Adv Mater 2001; 13:1099–102.
[22] Zhao DY, Yang PD, Melosh N, Feng JL, Chmelka BF, Stucky GD. Adv Mater 1998;10:1380–5.
[23] Wang J, Zhang CR, Feng J. Prog Chem 2005;17:1001–11.
[24] Cho AT, Pan FM, Chao KJ, Liu PH, Chen JY. Thin Solid Films 2005; 483:283–6.
[25] Morishige K, Tateishi N, Fukuma S. J Phys Chem B 2003;107:5177–81.
[26] Shi YF, Meng Y, Chen DH, Cheng SJ, Chen P, Yang TF, et al. Adv Funct Mater 2006;16:561–7.
[27] Vankelecom IFJ, VandenBroeck S, Merckx E, Geerts H, Grobet P, Uytterhoeven JB. J Phys Chem 1996;100:3753–8.
[28] Wang HT, Zhong W, Xu P, Du QG. Macromol Mater Eng 2004; 289:793–9.
[29] Ishikawa T, Matsuda M, Yasukawa A, Kandori K, Inagaki S, Fukushima T, et al. J Chem Soc Faraday Trans 1996;92:1985–9.
[30] Luan Z, He H, Zhou W, Klinowski J. J Chem Soc Faraday Trans 1998; 94:979–83.
[31] Caravajal GS, Leyden DE, Quinting GR, Macie GE. Anal Chem 1988; 60:1776–86.
[32] Mukherjee P, Laha S, Manda D, Kumar R. Stud Surf Sci Catal 2000; 129:283–6.
[33] Linde HG. J Polym Sci Polym Chem Ed 1982;20:1031–41.
[34] Yamada T, Ueda T, Kitayama TJ. Appl Phys 1982;53:4328–32.
[35] Hernandez-Torres J, Mendoza-Galvan A. J Non-Cryst Solids 2005; 351:2029–35.
[36] Wahab MA, Kim I, Ha CS. Polymer 2003;44:4705–13.
[37] Deligoz H, Yalcinyuva T, Ozgumus S, Yildirim S. J Appl Polym Sci 2006;100:810–8.
[38] Sharp KG. Adv Mater 1998;10:1243–8.
[39] Wen JY, Wilkes GL. Chem Mater 1996;8:1667–81.
[40] Mascia L, Kioul A. Polymer 1995;36:3649–59.
[41] Musto P, Ragosta G, Scarinzi G, Mascia L. Polymer 2004;45:1697–706.
[42] Chen BK, Chiu TM, Tsay SY. J Appl Polym Sci 2004;94:382–93.
[43] Im JS, Lee JH, An SK, Song KW, Jo NJ, Lee JO, et al. J Appl Polym Sci 2006;100:2053–61.
[44] Tsay SY, Chen BK, Chen CP. J Appl Polym Sci 2006;99:2966–72.
[45] Yen CT, Chen WC, Liaw DJ, Lu HY. Polymer 2003;44:7079–87.